

# Moisture-Resistant Perovskite Solar Cells: The Role of 1,1'-Methylenebispyridinium Dichloride in Enhancing Stability and Performance

Yong Hu<sup>a</sup>, Letian Dai<sup>a,b,\*</sup>, Tianyu Sun<sup>a</sup>, Haodan Shi<sup>a</sup>, Ying Xu<sup>a</sup>, Junyi Huang<sup>a</sup>,  
Xiongjie Li<sup>a</sup>, Shen Yan<sup>a</sup>, Mingkui Wang<sup>a,b,\*</sup>

<sup>a</sup> Wuhan National Laboratory for Optoelectronics, Huazhong University of Science and Technology, 1037 Luoyu Road, Wuhan 430074, Hubei, P. R. China

<sup>b</sup> Optics Valley Laboratory, Hubei 430074, China

E-mail: [ldai@hust.edu.cn](mailto:ldai@hust.edu.cn), [mingkui.wang@mail.hust.edu.cn](mailto:mingkui.wang@mail.hust.edu.cn).

## Materials

The etched indium tin oxide (ITO) glass sheets ( $R_{\square} \approx 8 \Omega/\text{sq}$ ) were purchased from Advanced Election Technology CO., Ltd (Yingkou, China). Methylammonium Iodide (MAI, 99.5%), Formamidinium iodide (FAI, 99.9%), Lead Iodide ( $\text{PbI}_2$ , 99.9%), methylammonium chloride (MACl, 99.9%), Cesium chloride, ( $\text{CsCl}$ , 99.9%), 2, 2'', 7, 7''-Tetrakis [N, N-di(4-methoxyphenyl) amino]-9, 9''-Spirobifluorene (Spiro-OMeTAD, 99.9%), 4-tert-butyl pyridine (4-tBP, 96%) and bis (trifluoromethyl sulfonyl)-imide lithium salt (Li-TFSI) were purchased from Xi'an Yuri Solar Co., Ltd.  $\text{SnO}_2$  (Tin (IV) oxide, 15% in  $\text{H}_2\text{O}$ ) colloidal dispersion liquid was purchased from Alfa

Aesar. Dimethyl sulfoxide (DMSO, 99.9%), N, N-dimethylformamide (DMF, 99.9%), chlorobenzene (CB, 99.9%), and isopropanol (IPA, 99.9%) were purchased from Sigma-Aldrich. Pyridine hydrochloride (PyCl, 98%) and 2-Phenylethylamine hydrochloride (PEACl, 99.5%) were purchased from Macklin. Pyridine (99.5%) was obtained from Shanghai Aladdin Biochemical Technology Co., Ltd., and dichloromethane (99.5%) was procured from Sinopharm Chemical Reagent Co., Ltd.

### **Synthesis of DipyCl<sub>2</sub>**

Modified general procedure for the synthesis of bis(imidazolium) and bis(pyridinium) dichloride salts was followed, starting with pyridine (0.32 mL, 4.0 mmol, 1.0 equiv), CH<sub>2</sub>Cl<sub>2</sub> (0.77 mL, 12.0 mmol, 3.0 equiv) and DMSO (0.23 mL, 3.2 mmol, 0.8 equiv) at 100 °C for 48 hours. After cooling to room temperature, the heterogenous mixture was dissolved in MeOH (20 mL) and concentrated under vacuum, affording white solid. The resulting white solid was recrystallized three times with MeOH to obtain pure DipyCl<sub>2</sub> (purity 99.3%).

### **Experimental Section**

***Preparation of solutions:*** The SnO<sub>2</sub>-KCl solution was prepared by mixing 15% SnO<sub>2</sub> hydrocolloid solution with 5 mg·mL<sup>-1</sup> KCl solution at a volume ratio of 1:1. The mixed solution was stirred for 2 h, then filtered by a 0.22 μm syringe filter before use. To prepare a FA<sub>0.95</sub>Cs<sub>0.05</sub>PbI<sub>3</sub> precursor solution, PbI<sub>2</sub>, FAI, CsCl, MAI and MACl with a molar ratio of 1.1:0.95:0.05: 0.05 and 0.2 were dissolved in a mixed solvent of DMF and DMSO (v: v = 4: 1) to form a 1.1 M precursor solution. DiPyCl<sub>2</sub> was added to the

perovskite solution at different molar ratios relative to lead iodide (0, 0.05, 0.10, 0.20, 0.50, 1.00, and 2.00 mol%). The perovskite precursor solution was stirred for at least 12 h, then filtered by a 0.22  $\mu\text{m}$  syringe filter before use. For the hole transport layer, 72.3 mg Spiro-OMeTAD was dissolved in 1 mL chlorobenzene, stirred for 20 min, then 17.5  $\mu\text{L}$  Li-TFSI (520 mg Li-TFSI dissolved in 1 mL acetonitrile) and 28.5  $\mu\text{L}$  t-BP was added. The Spiro-OMeTAD solution was obtained by stirring at room temperature for 12 h.

***Fabrication of planar-structure solar cell:*** ITO-glasses were sequentially cleaned in detergent, deionized water, acetone, and alcohol for 20 minutes. The glasses were then treated with ultraviolet ozone for 30 minutes. First, a  $\text{SnO}_2$  layer was deposited on the ITO substrate by spin-coating the prepared  $\text{SnO}_2$ -KCl solution at 4000 rpm for 20 s, and then annealed at 150  $^\circ\text{C}$  for 30 minutes. The substrates were then treated with UV ozone for 30 minutes before starting the next procedures. The perovskite precursor was spin-coated on the  $\text{SnO}_2$  substrates with a two-step process method. The first step was 1000 rpm for 5 s with an acceleration of 200  $\text{rpm s}^{-1}$ . The second step was 4,000 rpm for 30 s with an acceleration of 4,000  $\text{rpm s}^{-1}$ . 15 s after the start of the second spin step, 200  $\mu\text{L}$  of CB anti-solvent was added dropwise. The perovskite film was successively heated to 100  $^\circ\text{C}$  for 60 minutes and at 140  $^\circ\text{C}$  for 10 minutes. To deposit the hole transport layer, we spin-coated the prepared Spiro-OMeTAD precursor onto the perovskite film surface (5000 rpm, 20 s). Finally, a 100 nm Ag electrode was deposited using a thermal evaporator to complete the fabrication of PSC devices.

***Characterization:*** We utilized a xenon light source solar simulator (450W, Oriel,

model 9119) equipped with an AM 1.5G filter (Oriel, model 91192) to deliver an irradiance of  $100 \text{ mW}\cdot\text{cm}^{-2}$  at the surface of the solar cells. The photocurrent-voltage (J-V) characteristics of the  $0.04 \text{ cm}^2$  size devices were measured under these conditions by applying an external potential bias to the devices and measuring the resulting photocurrent using a Keithley model 2400 digital source meter. The IPCE values for light-bias free devices were measured in the wavelength range of 300 to 900 nm using IQE200B, Oriel. The Thickness was measured by a stylus profiler (DektakXT, Bruker, America). Carbon NMR (C-NMR) spectroscopy was performed by Ascend™ 600 MHZ (Bruker, Switzerland). Liquid chromatography-mass spectrometry (LC-MS) was conducted at 1100 LC/MSD Trap (Agilent, America). The surface morphology was examined by using field-emission scanning electron microscopy (FSEM, Nova NanoSEM 450). High resolution transmission Electron Microscope (HRTEM) measurement was carried out by Talos F200X. Atomic Force Microscope (AFM) and Kelvin Probe Force Microscopy (KPFM) experiments were obtained on a SPM9700 (Shimadzu, Japan), with a nominal spring constant of  $2.8 \text{ N m}^{-1}$ . The tip was calibrated using a highly ordered pyrolytic graphite (HOPG) sample. X-ray diffraction (XRD) pattern was recorded by utilizing a Shimadzu XRD-6100 diffractometer with  $\text{Cu K}\alpha$  radiation. UV-vis absorption spectra were recorded using a PE950 spectrophotometer. The samples were uniformly deposited on glass substrates following the identical procedure used for device fabrication. X-ray photoelectron spectroscopy (XPS) was conducted using a photoelectron spectrometer (AXIS-ULTRA DLD-600W, Kratos, Shimadzu, Japan). Contact angle was obtained on a SDC-200Z (Sindin, China).

Time-resolved photoluminescence decays (TRPL) were measured at 800 nm with a 478 nm light pulse as excitation by Delta Flex Fluorescence Lifetime System (Horiba Scientific Com., Japan). The decay kinetics were determined by fitting with a bi-exponential decay profile described by the function:

$$I_{PL}(t) = A_1 e^{-K_1 t} + A_2 e^{-K_2 t} + C \quad (1)$$

with the average carrier lifetime given by:

$$\frac{1}{\tau_{ave}} = \frac{A_1 \tau_1 + A_2 \tau_2}{A_1 \tau_1^2 + A_2 \tau_2^2} \quad (2)$$

where  $\tau_1 = \frac{1}{k_1}$  and  $\tau_2 = \frac{1}{k_2}$ .

**DFT calculations:** Density functional theory calculations used the Vienna Ab initio Simulation Package (VASP). The projected augmented wave (PAW) method and the Perdew–Burke–Ernzerhof (PBE) functional within the generalized gradient approximation (GGA) were employed to describe the interaction between ion-cores and valence electrons and exchange–correlation effects, and an energy cutoff of 500 eV was set for the plane-wave function expansion. The van der Waals (vdW) dispersion correction was described by the DFT-D3 correction. The first Brillouin zone was sampled on a  $2 \times 3 \times 1$  gamma ( $\Gamma$ )-centered k-space mesh for structural relaxation and static calculations. The atomic positions of all slabs were relaxed until the total energy changes were less than  $1.0 \times 10^{-5}$  eV and the maximum force relaxed down to 0.05 eV·Å<sup>-1</sup>.

The energy barrier associated with the deprotonation-erosion process was calculated for the free state  $\text{Py}^+$  and  $\text{PEA}^+$  cations before they are absorbed into the perovskite surface, as shown in the equation:  $E_f = [E_{[M]} + E_{[HI]}] - [E_{[M^+] + E_{[I^-]}]$ , where  $E_{[M]}$  denotes the total energy of a deprotonated  $\text{Py}^+/\text{PEA}^+$ ,  $E_{[HI]}$  denotes the total energy of a HI molecule,  $E_{[M^+]}$  denotes the total energy of a  $\text{Py}^+/\text{PEA}^+$  cations, and  $E_{[I^-]}$  denotes the total energy of an I ion. The formation energies of iodine vacancy on perovskite surface with and without the presence of  $\text{Dipy}^{2+}$  cations were also calculated. The  $\text{pK}_a$  values of various cations are calculated with the MarvinSketch software.

To calculate the adsorption formation energy on the perovskite facet, the following expression was used:  $E_{\text{ads}} = E_{[\text{Dipy}]^{2+}/\text{sur}} - E_{[\text{Dipy}]^{2+}} - E_{\text{sur}}$ .  $E_{[\text{Dipy}]^{2+}/\text{sur}}$ ,  $E_{[\text{Dipy}]^{2+}}$  and  $E_{\text{sur}}$  are the energy of the  $[\text{Dipy}]^{2+}$  cation adsorbed on the perovskite surface,  $[\text{Dipy}]^{2+}$  and the perovskite surface, respectively. Calculations of adsorption formation of  $\text{Dipy}^{2+}$  are based on the (100), (110) and (111) perovskite surfaces.

Calculations of adsorption formation of water are based on the pure perovskite and  $\text{Dipy}^{2+}/\text{perovskite}$  surfaces.

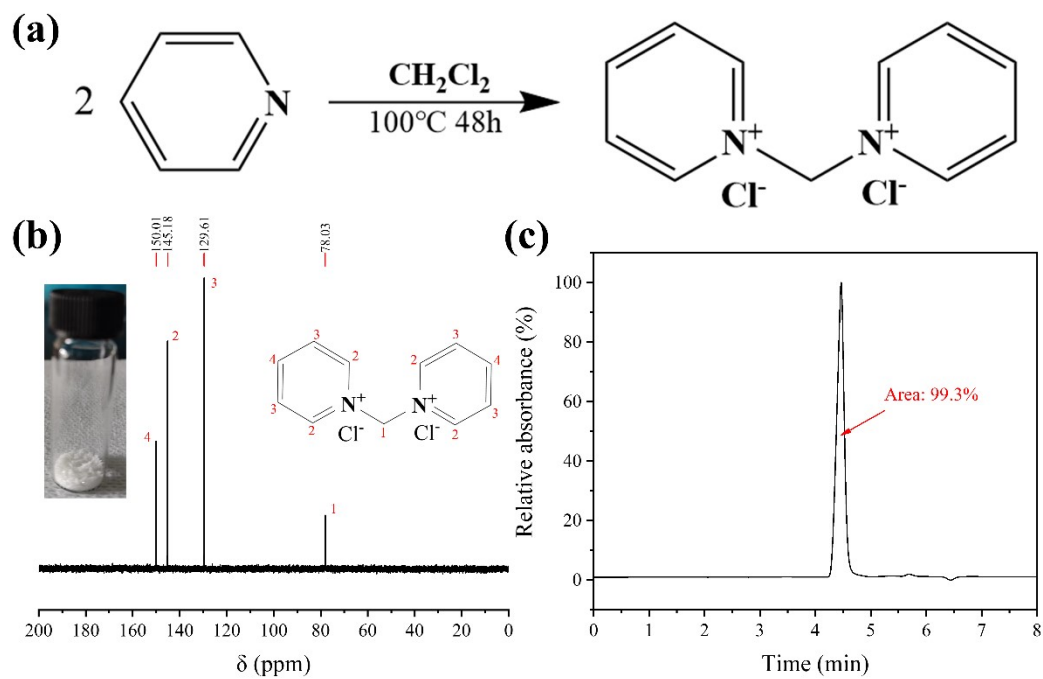


**Figure S1.** Synthesis of pure DipyCl<sub>2</sub>. (a) Synthesis path of DipyCl<sub>2</sub>, (b) Photograph of DipyCl<sub>2</sub> after three recrystallizations in MeOH and C-NMR spectrum of DipyCl<sub>2</sub> in D<sub>2</sub>O, (c) LC-MS of DipyCl<sub>2</sub> dissolved in a mixed solvent (2:98 in volume) of MeOH and deionized water containing 0.10% formic acid.

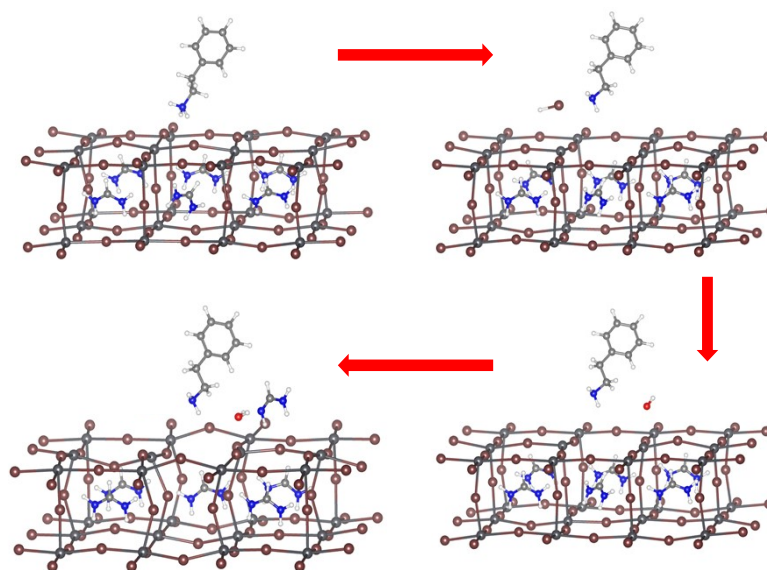


**Figure S2.** DFT simulations of the reaction and decomposition at the FAPbI<sub>3</sub> perovskite/PEA<sup>+</sup> interface

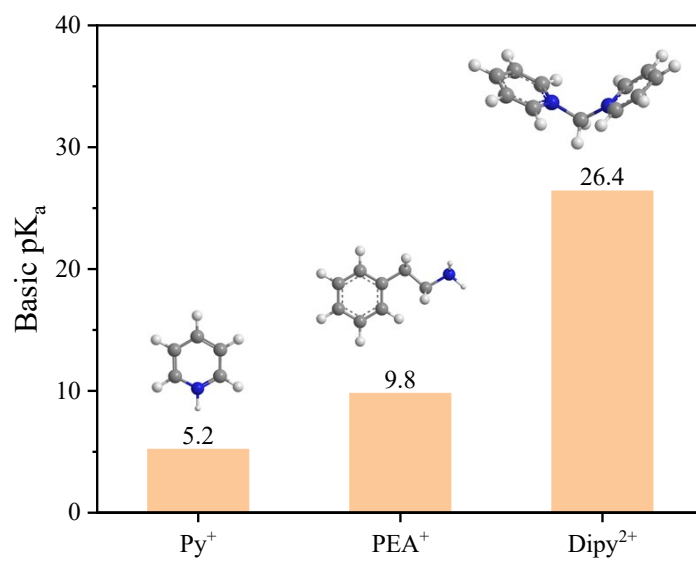


**Figure S3.** Structures of Py<sup>+</sup>, PEA<sup>+</sup> and Dipy<sup>2+</sup> and corresponding pK<sub>a</sub> values.

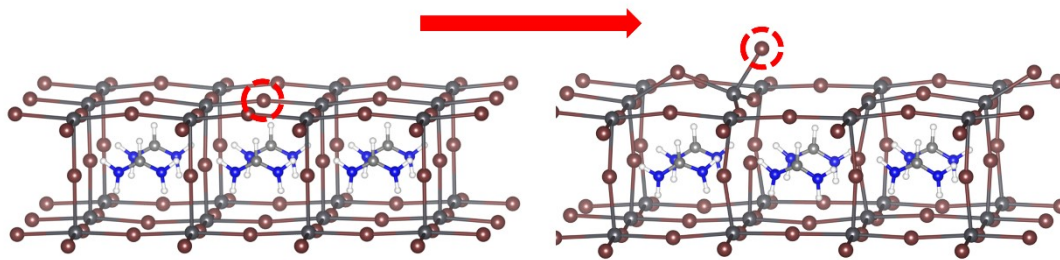


**Figure S4.** DFT simulations of the formation of iodine vacancy at the pure FAPbI<sub>3</sub> perovskite surface.

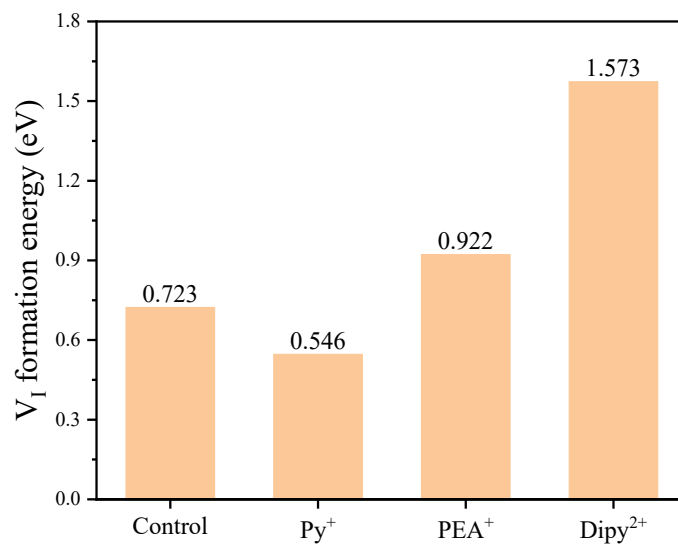
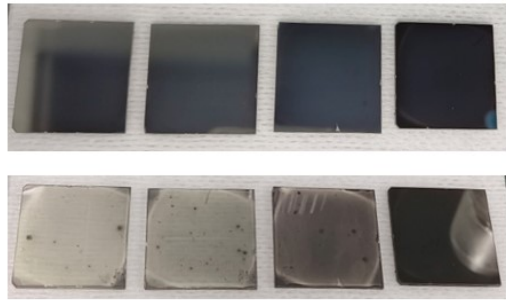


**Figure S5.** The formation energy of iodine vacancy ( $V_I$ ) on the pure,  $Py^+$ ,  $PEA^+$ ,  $Dipy^{2+}$  absorbed  $FAPbI_3$  perovskite surface, calculated by DFT.

Control PyCl- PEACl- DipyCl<sub>2</sub>-



12 h in air(25°C 60%±10 RH)

**Figure S6.** Photos of air-aged Control, PyCl-, PEACl- and DipyCl<sub>2</sub>-treated perovskite films before (top) and after (bottom) aging.

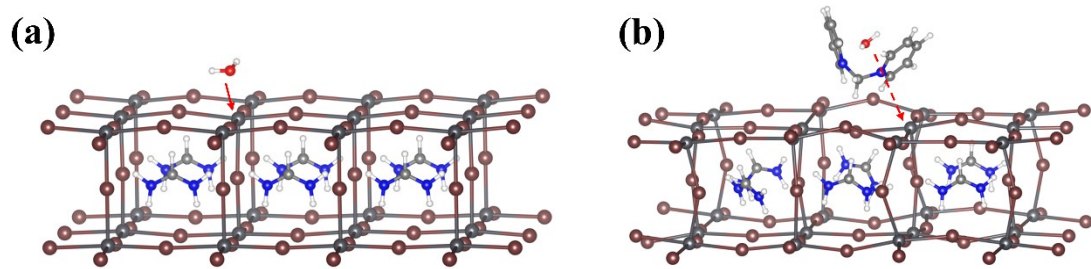


**Figure S7.** Adsorption energy of water molecules with FAPbI<sub>3</sub> surface calculated by DFT. (a) pure FAPbI<sub>3</sub>, (b) Dipy<sup>2+</sup>/ FAPbI<sub>3</sub>

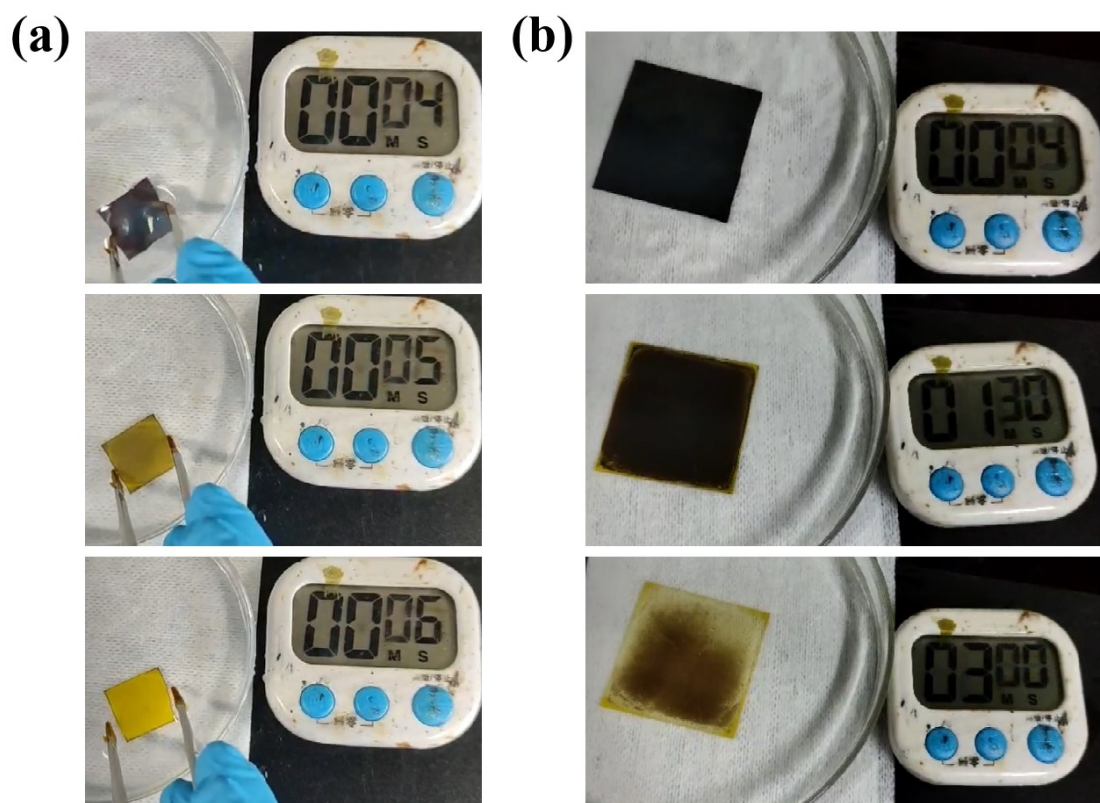


**Figure S8.** Photographs showing the color change of perovskite films placed in water over time, comparing (a) the control sample without additives to (b) the sample with 2.00 mol% additive.

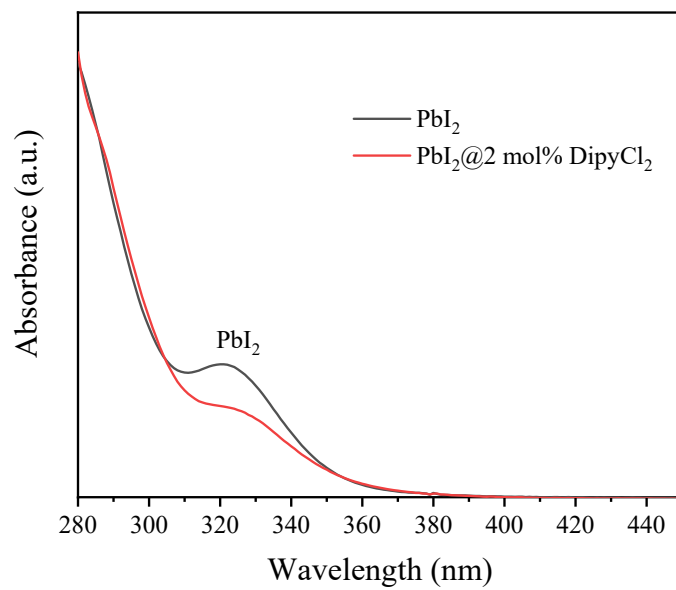


**Figure S9.** UV-vis absorption spectra of  $\text{PbI}_2$  and  $\text{PbI}_2$  with 2.00 mol% additive.

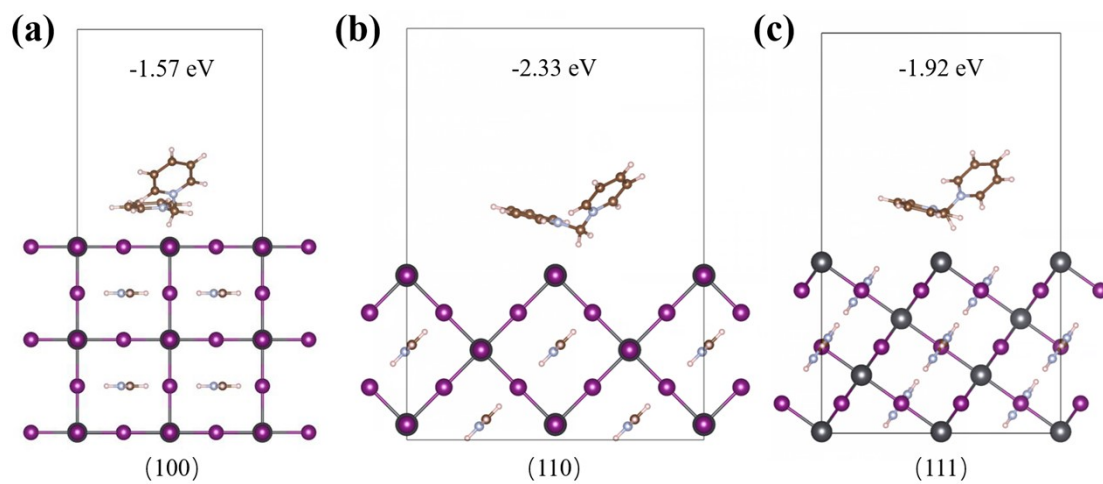


**Figure S10.** Calculated models of Dipy<sup>2+</sup> adsorbed on different facets of FAPbI<sub>3</sub> and the corresponding adsorption energies. (a) (100), (b) (110), (c) (111).

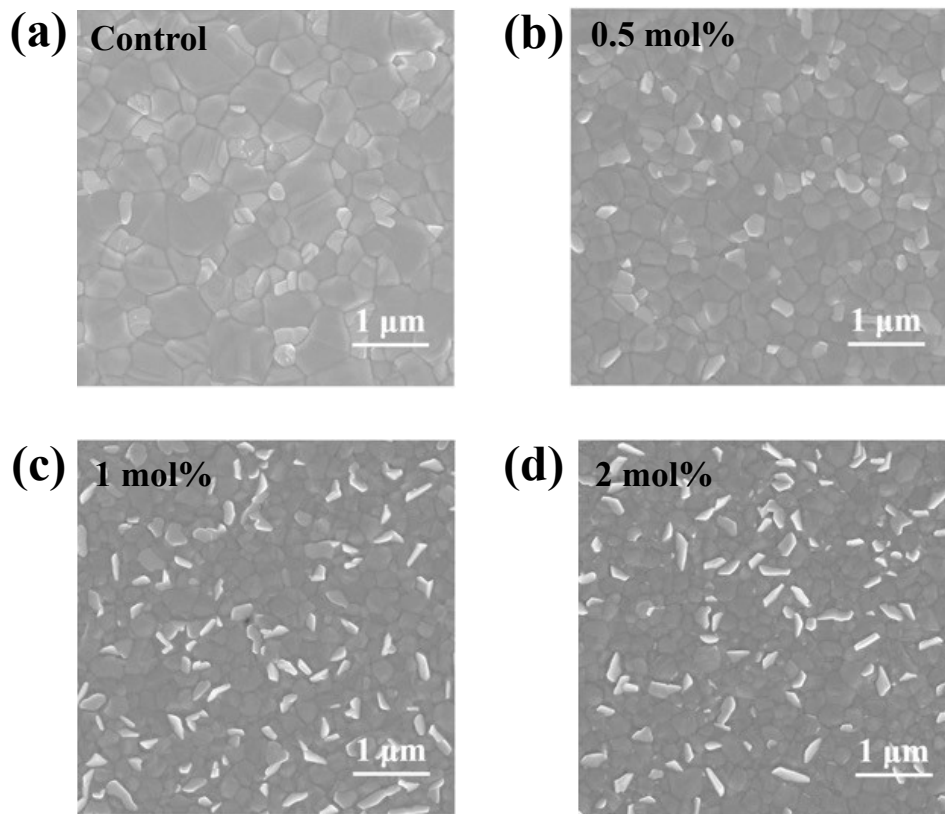


**Figure S11.** SEM images of (a) the control perovskite film and those with additives at the percentage of (b) 0.50 mol%, (c) 1.00 mol%, and (d) 2.00 mol%. Scale bar 1 μm.

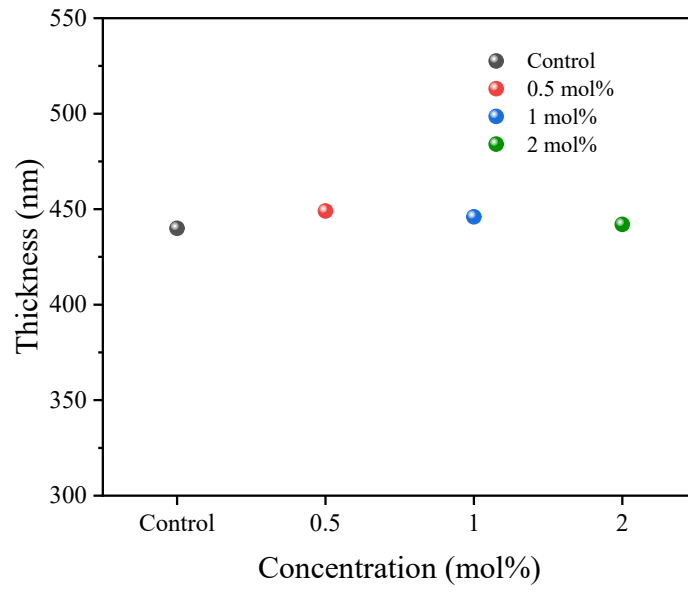


**Figure S12.** Thickness of the perovskite films on glass substrates for the control sample and the samples with additives at a percentage of 0.50 mol%, 1.00 mol% and 2.00 mol%.

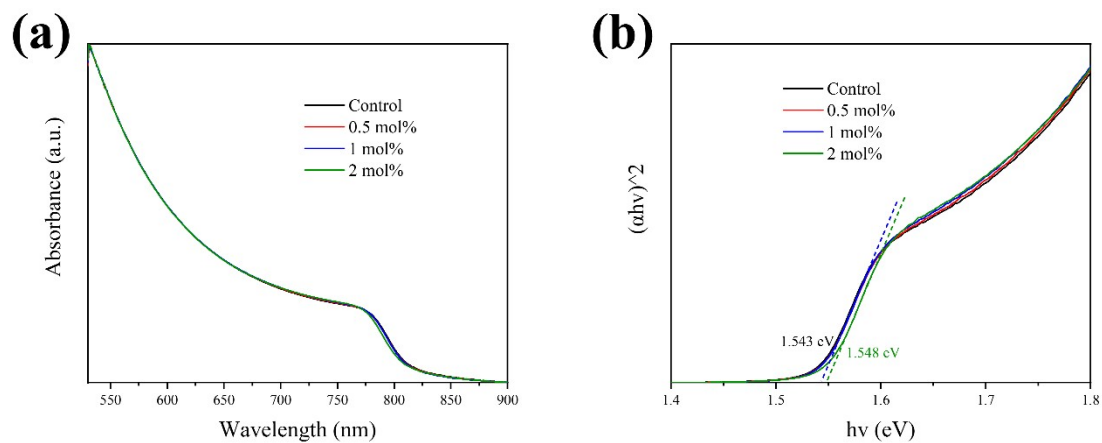


**Figure S13.** (a) UV-vis absorption spectra and (b) Tauc-Plot fitting curves for the control sample and the samples with additives at a percentage of 0.50 mol%, 1.00 mol% and 2.00 mol%.

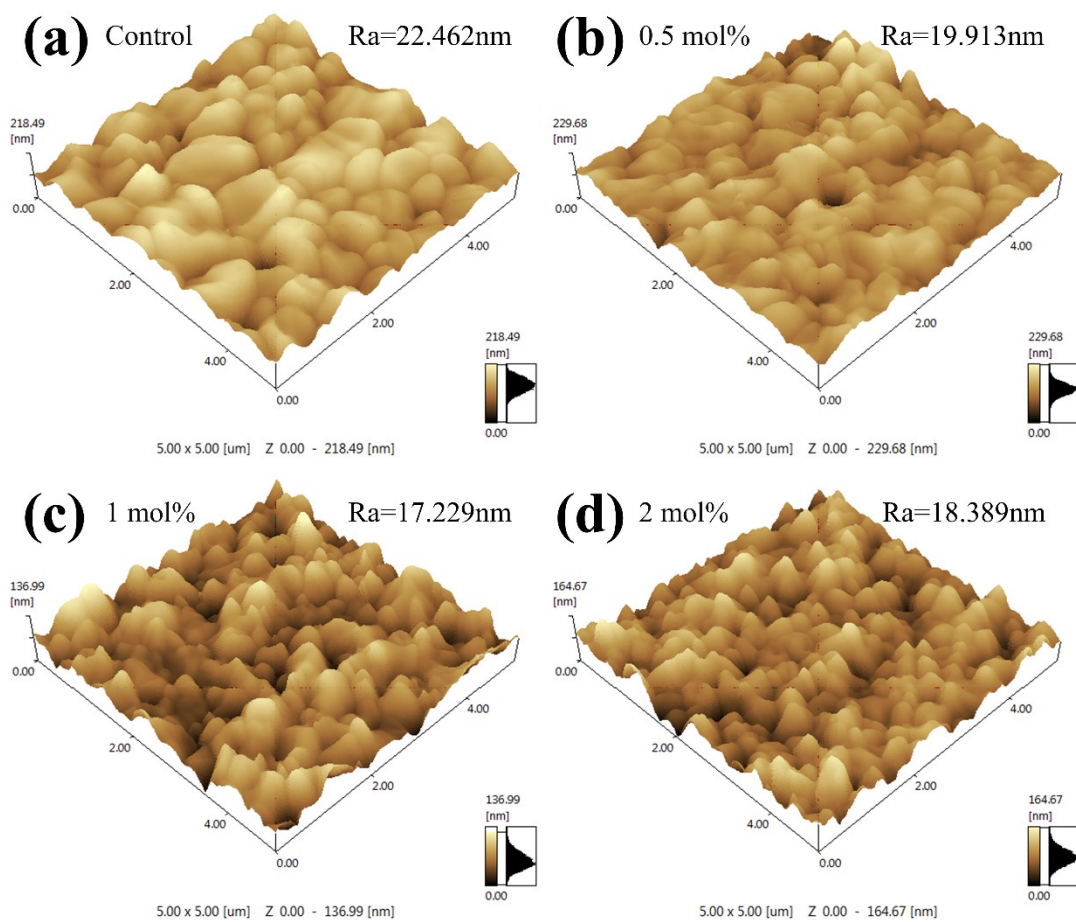


**Figure S14.** AFM 3D maps of (a) the control perovskite film and those with additives at the percentage of (b) 0.50 mol%, (c) 1.00 mol%, and (d) 2.00 mol%.

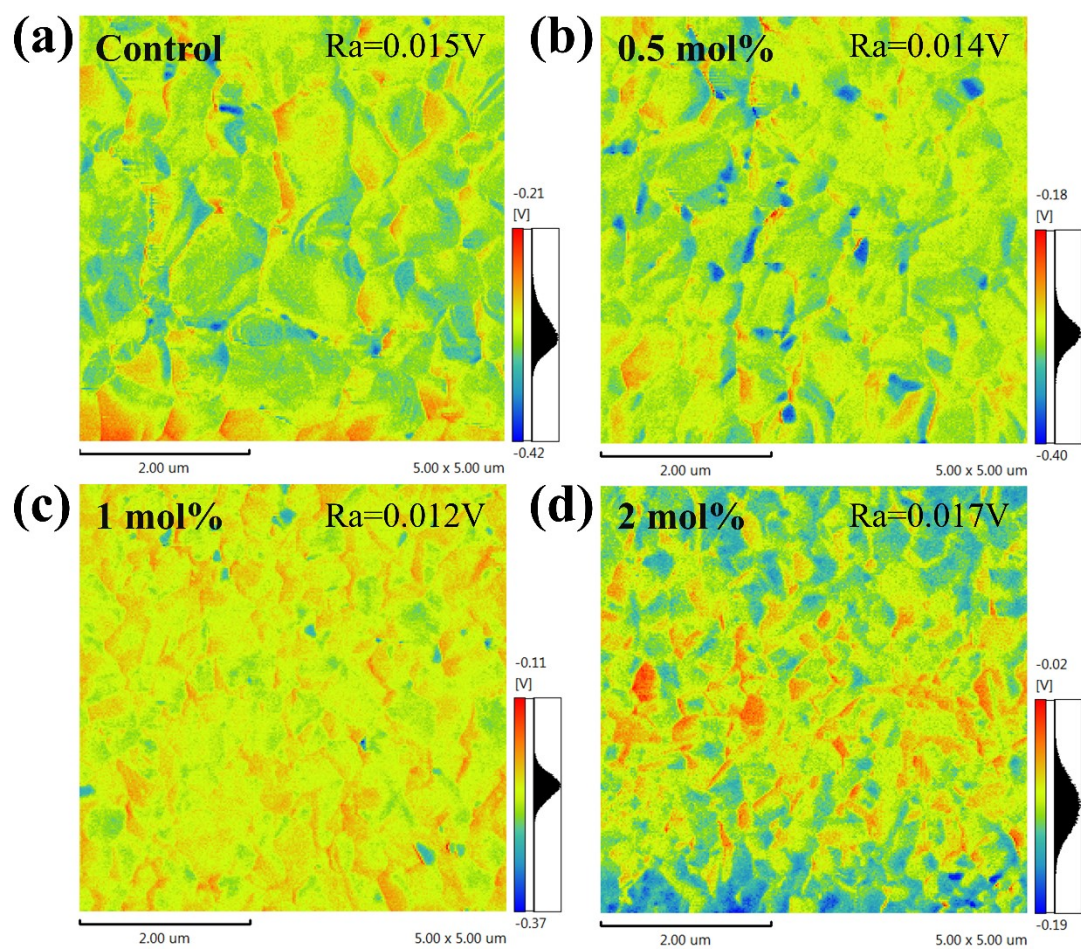


**Figure S15.** KPFM potential maps of (a) the control perovskite film and those with additives at the percentage of (b) 0.50 mol%, (c) 1.00 mol%, and (d) 2.00 mol%. Scale bar 2  $\mu\text{m}$ .

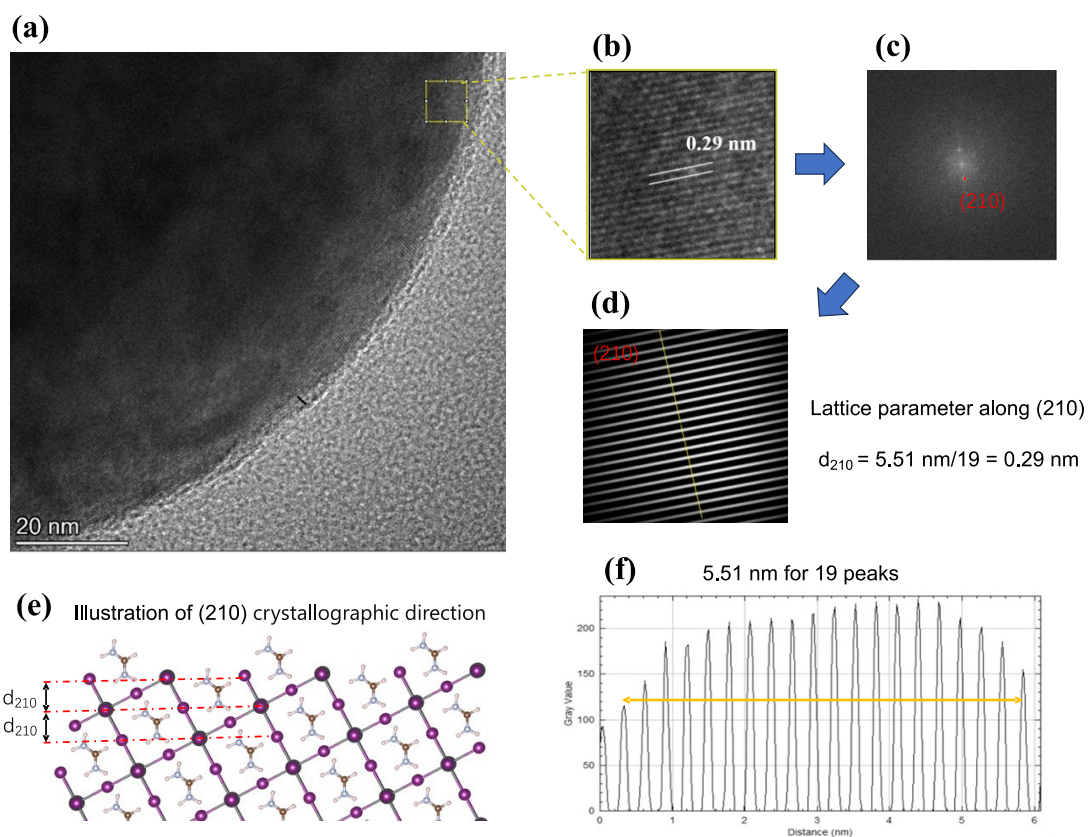


**Figure S16.** (a) HRTEM image in a large area for a perovskite grain with 2.00 mol% DipyCl<sub>2</sub> additive, (b) the HRTEM image, and (c) the corresponding FFT pattern for the selected area. Scale bar 20 nm. (d) The inverse FFT image of the selected spot (210) in the FFT pattern image. (e) A schematic image of  $\alpha$ -phase FAPbI<sub>3</sub> crystal structure to emphasize the lattice along (210). (f) Image pixel intensity along the bright line perpendicular to the bright grids to determine the lattice parameter along (210).

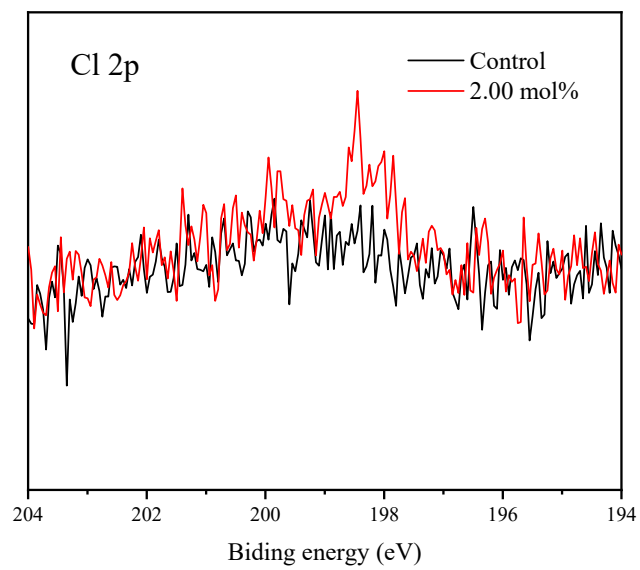


**Figure S17.** XPS for Cl 2p analysis of control and 2.00 mol% additive sample.

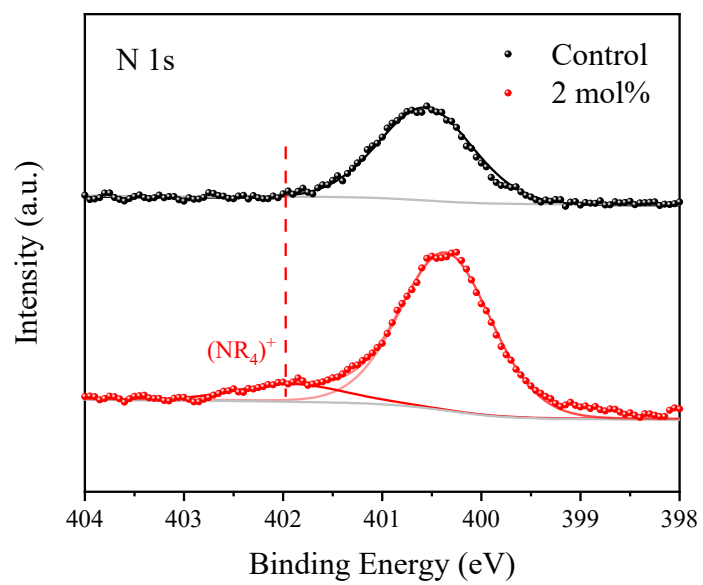


**Figure S18.** XPS for N 1s analysis of control and 2.00 mol% additive sample.

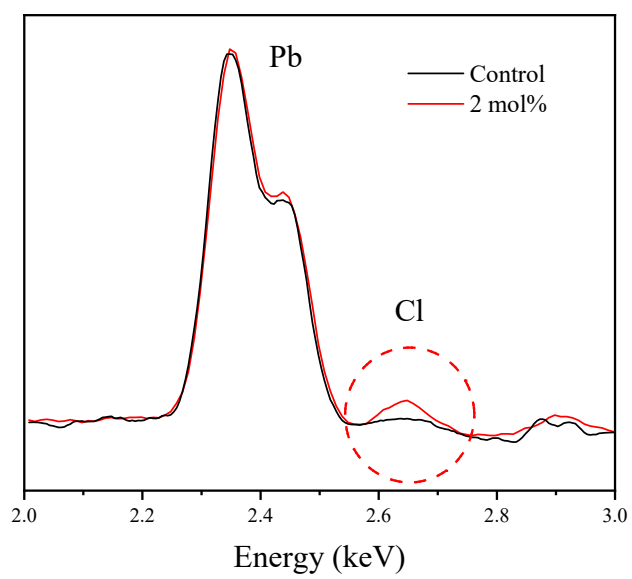


**Figure S19.** Energy dispersive spectroscopy for Cl analysis of control and 2.00 mol% additive sample.

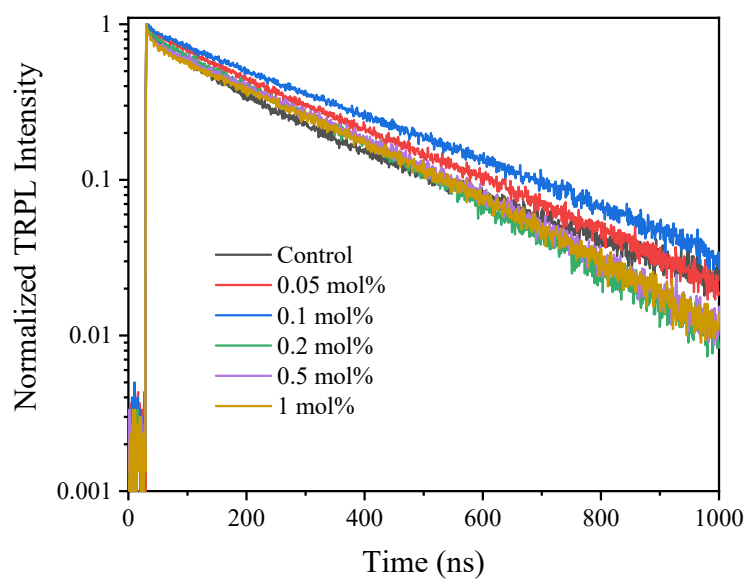


**Figure S20.** TRPL for the control sample and the samples with additives at a percentage of 0.05 mol%, 0.10 mol% and 0.20 mol% 0.50 mol%, and 1.00 mol%.

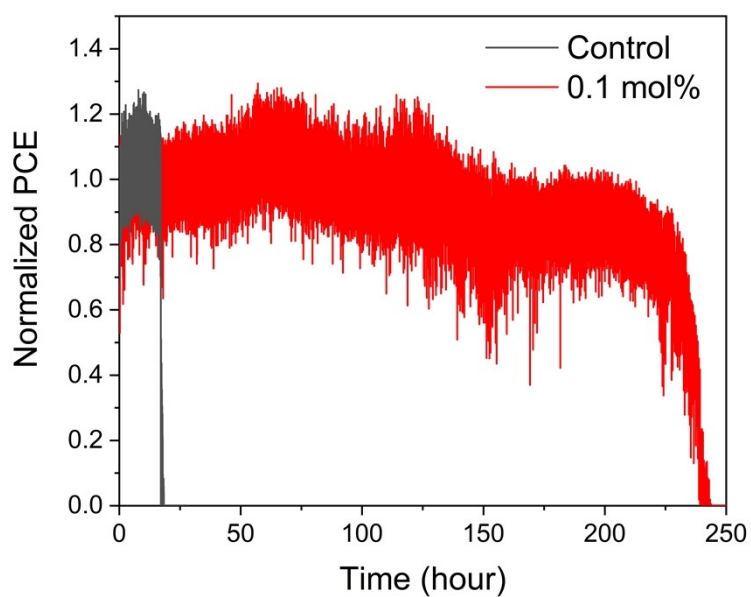


**Figure S21.** Stabilized maximum power point (MPP) values recorded for the control and 0.10 mol% additive-based devices without encapsulation under continuous light irradiation with a white LED lamp at  $100 \text{ mW cm}^{-2}$  in air environment ( $20 \pm 5 \text{ }^\circ\text{C}$  and  $60 \pm 10\%$  relative humidity).

**Table S1.** The fitting results from TRPL characterization of perovskite films with different amounts of DipyCl<sub>2</sub> additive extracted from the Figure S16.

Films	$\tau_1$ (ns)	A1 (%)	$\tau_2$ (ns)	A2 (%)
Control	95.45	0.52	312.99	0.48
0.05 mol%	42.05	0.20	277.66	0.80
0.10 mol%	28.47	0.20	296.41	0.80
0.20 mol%	11.27	0.67	259.16	0.33
0.50 mol%	8.73	0.87	249.69	0.13
1.00 mol%	8.57	0.90	249.21	0.10